Laminar burning characteristics of ammonia/hydrogen/air mixtures with laser ignition

Wang, Ning; Huang, Shuai; Zhang, Zhifei; Li, Tie; Yi, Ping; Wu, Dawei; Chen, Gen

DOI:
10.1016/j.ijhydene.2021.07.063

Document Version
Peer reviewed version

Citation for published version (Harvard):
Wang, N, Huang, S, Zhang, Z, Li, T, Yi, P, Wu, D & Chen, G 2021, 'Laminar burning characteristics of ammonia/hydrogen/air mixtures with laser ignition', *International Journal of Hydrogen Energy*, vol. 46, no. 62, pp. 31879-31893. https://doi.org/10.1016/j.ijhydene.2021.07.063

Laminar burning characteristics of ammonia/hydrogen/air mixtures with laser ignition

Ning Wang[1], Shuai Huang[1, 2*], Zhifei Zhang[1], Tie Li[1, 2*], Ping Yi[1, 2], Dawei Wu[3], Gen Chen[3]

1. State Key Laboratory of Ocean Engineering, Shanghai Jiao Tong University
2. Institute of Power Plants and Automation, Shanghai Jiao Tong University
3. Department of Mechanical Engineering, University of Birmingham

*Corresponding Address: 800 Dongchuan Rd., Shanghai, PR China, 200240;
Tel.: (86)21-3420-8348; *E-mail*: zzdett@163.com； litie@sjtu.edu.cn

ABSTRACT

Ammonia, as a zero-carbon fuel, is drawing more and more attention. The major challenge of using ammonia as a fuel for the combustion engines lies in its low chemical reactivity, and therefore more fundamental researches on the combustion characteristics of ammonia are required to explore effective ways to burn ammonia in engines. In this study, the laminar burning characteristics of the premixed ammonia/hydrogen/air mixtures are investigated. In the experiment, the laser ignition was used to achieve stable ignition of the ammonia/air mixtures with an equivalence ratio range from 0.7 to 1.4. The propagating flame was recorded with the high-speed shadowgraphy. Three different processing methods were introduced to calculate the laminar burning velocity with a consideration of the flame structure characteristics induced by the laser ignition. The effects of initial ambient pressure (0.1 MPa-0.5 MPa), equivalence ratio (0.7-1.4), hydrogen fraction (0-20%) on the laminar burning velocity were investigated under the initial ambient temperature of 360K. The state-of-the-art kinetic models were used to calculate the laminar burning velocities in the CHEMKIN-pro software. Both the simulation and experimental results show that the laminar burning velocity of the ammonia mixtures increases at first, reaches the peak around ϕ of 1.1, and then decreases with the equivalence ratio increasing from

0.7 to 1.4. The peak laminar burning velocities of the ammonia mixture are lower than 9 cm/s and are remarkably lower than those of hydrocarbon fuels. The laminar burning velocity of the ammonia mixture decreases with the increase of the initial ambient pressure, and it can be drastically speeded up with the addition of hydrogen. While the models except for those by Miller and Bian can give reasonable predictions compared to the experimental results for the equivalence ratio from 0.7 to 1.1 in the ammonia (80%)/hydrogen (20%)/air mixtures, all the kinetic models overpredict the experiments for the richer mixtures, indicating further work necessary in this respect.

Keywords: Ammonia; Hydrogen; Laser ignition; Combustion; Laminar burning velocity

1. Introduction

With the large-scale use of fossil fuels, environmental problems such as the greenhouse effect have become increasingly serious. In 2015, nearly 200 parties to the United Nations Framework Convention on Climate Change agreed to adopt the Paris Agreement, striving to achieve the net zero emissions of greenhouse gases in the second half of this century [1]. The development of new combustion technologies and the utilization of clean energy have become more urgent and important. As clean fuels that do not contain carbon element, ammonia and hydrogen are receiving more and more attention.

Ammonia can be used as a hydrogen storage fuel. In the ammonia molecule, the mass content of the hydrogen element reaches 17.7%. Compared with hydrogen, ammonia is of much lower chemical reactivity, and can be liquefied when the pressure reaches 0.857 MPa at 20°C. These properties facilitate a vast potential for the safe and convenient storage as well as transportation [2]. In terms of ammonia production, a complete ammonia production industry has been established worldwide, which are being constantly optimized to reduce carbon emissions in the ammonia production processes [3].

In recent years, green ammonia production technologies using clean energy such as solar and wind energy have gradually been promoted and used [4, 5]. Moreover, the specific energy of ammonia is 22.5 MJ/kg, which can reach a level comparable to that of some carbon-containing fuels. For example, the specific energy of low-grade coal is about 20 MJ/kg [6]. In terms of the engine applications, the octane number of ammonia is high, and it will not cause severe knocks when working in the spark ignition engines with high compression ratios, thereby a high efficiency can be expected.

However, on account of the low chemical reactivity of ammonia, its ignition temperature is high, the flammable range is narrow, the combustion intensity is weak, the flame propagation speed is slow during the combustion processes, and the heat release is slow, which limit its further popularization and application to some extent [7]. In addition, a significant amount of NO_x is inevitably produced during the combustion of ammonia, which is also one of the current challenges. Therefore, more fundamental researches are needed on the combustion of ammonia in order to better understand and utilize it.

The chemical reaction mechanism of ammonia combustion has been updated and revised since last century. In the early days, Miller et al. [8] and Bian et al. [9] studied the components in the laminar flame through ammonia combustion experiments. They developed the mechanisms of ammonia oxidation, and clarified the main generation paths of some intermediate products (such as NO, N_2O, etc.). Lindstedt et al. [10] studied the planar laminar premixed flame with different proportions of the ammonia/hydrogen/oxygen mixtures. The mechanism involved 22 chemical components and 95 elementary reactions, but it did not simulate the flame structure, which resulted in certain limitations. In recent years, more and more researchers are participating in the study of the ammonia combustion mechanism. Tian et al. [11], Okafor et al. [12], Mei et al. [13], Shrestha et al. [14] and Stagni et al. [15]

have updated the kinetic models of ammonia chemical reactions, respectively. Goldmann et al. [16] developed the laminar burning velocity correlations with the ambient pressure, temperature and gas composition for ammonia/hydrogen/air mixtures based on the Mathieu's mechanism [17] and experimental data in literature. However, different kinetic models lead to big differences in predictability of the ammonia combustion characteristics, such as the ignition delay, the laminar burning velocity, the product concentration and so on. Therefore, more systematic experimental data are required to modify these kinetic models under more complete conditions.

The laminar burning velocity is crucial to evaluate the combustion for both fundamental research and practical application [18], which can characterize the chemical reactivity of combustibles. Pfahl et al. [19] and Takizawa et al. [20] successively explored the speed of the spherical flame propagating outward when the ammonia/air mixtures were burned at 0.1 MPa. The results confirmed that the laminar burning velocity of ammonia is lower than that of some small molecular hydrocarbon fuels under the same conditions. Hayakawa et al. [21] used a capacitor device to make the spark plug instantly generate sufficient ignition energy to ignite the ammonia/air mixtures. The results showed that the laminar burning velocity decreased as the initial ambient pressure became higher. In addition, the recent study [13, 22-24] showed that an appropriate increase in oxygen concentration, hydrogen fractions or higher initial fuel temperature and can improve the ammonia combustion processes.

A wide range of equivalence ratios are usually encountered in practical combustion devices. The diffusion combustion is generally acknowledged to be an effective way in compression ignition engines, turbine engines, boiler combustors and linear free piston engines, where ammonia has great potential to be used. In recent years, the authors in literatures [13, 20, 21, 23-26] have used electric spark to ignite the premixed ammonia/air gas, but the equivalence ratio range they researched was

limited from 0.9 to 1.3. Though in the earlier studies, Zakaznov et al. (1978) [27] and Ronney et al. (1988) [28] reported the laminar burning velocities under the richer conditions, they made a very complicated modification to the ignition device that seems not applicable in practicle devices. Therefore, it is very difficult to use spark ignition to achieve successful ignition within a wide range of equivalence ratio. There should be a better choice of ignition method and the previous experimental data need to be updated in the modern experimental environment.

In this study, the laser ignition is used to broaden the ignitable range of ammonia. The laminar burning characteristics of ammonia are investigated in a wider range of equivalence ratios. Laser ignition is realized by focusing the laser beam with a certain energy into the combustible mixture, and then induce hot plasma. After that, an initial flame kernel forms and the combustion process begins. The electric spark ignition often encounters the electrode ablation and quenching especially at the early stage of the flame development. Compared with the electric spark, the laser ignition, as the “non-intrusive ignition”, would not interfere with the local flow field. It can reduce the heat transfer loss and make the flame propagation more stable during the initial stage [29]. For some combustibles with the low chemical reactivity and weak combustion intensity, such as ammonia, it is easier to achieve stable initial flame by using laser ignition. In addition, laser ignition is also characterized by the flexible and variable ignition position, short ignition delay, precise ignition time control, improved combustion process to reduce emissions, and expanded lean burn limit of the mixture [30]. When it is used in the engine, the auto-ignition and backfire from gas fuelled engine can be overcome. It is also proved that the maximum in-cylinder pressure, the maximum rate of pressure rise and heat release rate are higher with laser ignition, such that the engine performance parameters for laser ignition were superior than spark ignition [31, 32]. However, the existing researches with laser ignition are mostly

111 focused on hydrocarbon fuels, and there are few reports on the ammonia mixtures, while the stable
112 ignition is one of the challenges for ammonia mixtures.

113 The objective of this work is to deepen the study of the laminar flame propagation in the
114 ammonia/hydrogen/air mixtures under a wider equivalence ratios range with laser ignition. This paper
115 investigates the laminar burning characteristics of the premixed ammonia/hydrogen/air mixtures with
116 the experiments and simulations. In the experiment, the laser ignition is used to successfully ignite the
117 ammonia/air mixtures within a wide range of an equivalence ratio range from 0.7 to 1.4. The structure
118 of this paper is as follows. After the Introduction, the experimental apparatus and simulation methods
119 are firstly described, and then three different processing methods considering the flame structure
120 characteristics induced by laser ignition are introduced. In the results and discussion part, the flame
121 morphology changing with time after the laser ignition is analyzed. Then the experimental and
122 simulation results of the laminar burning velocity under different conditions are compared. Moreover,
123 the changes of the flame thickness under different conditions are evaluated. Finally, the main
124 conclusions are summarized.

125 **2. Experimental and numerical methods**

126 *2.1. Experimental methods*

127 Fig. 1 displays the experimental setup used in this study. The internal volume of the CVCC is 0.9
128 litre, which is approximately a cube with a side length of 97 mm. Three optical windows with a
129 diameter of 90 mm on the CVCC were used to set the laser and shadowgraph light path, and the other
130 side of the CVCC were equipped with the inlet and exhaust pipe, the temperature sensor and pressure
131 sensors. In addition, a mixing fan was installed on the top side of the CVCC to make the mixture as

homogeneous as possible and it stopped 30 seconds before the ignition. An electric heater combined with a temperature controller was employed to keep the gas temperature constant at 360 K. The air and ammonia or ammonia/hydrogen mixtures from the high-pressure gas cylinders were respectively charged into the CVCC to create a combustible mixture. The various equivalence ratios of the ammonia/hydrogen/air mixtures can be obtained by controlling the partial pressure of the components. During the intake process, a piezoresistive sensor was used to ensure the accurate measurement of the pressure.

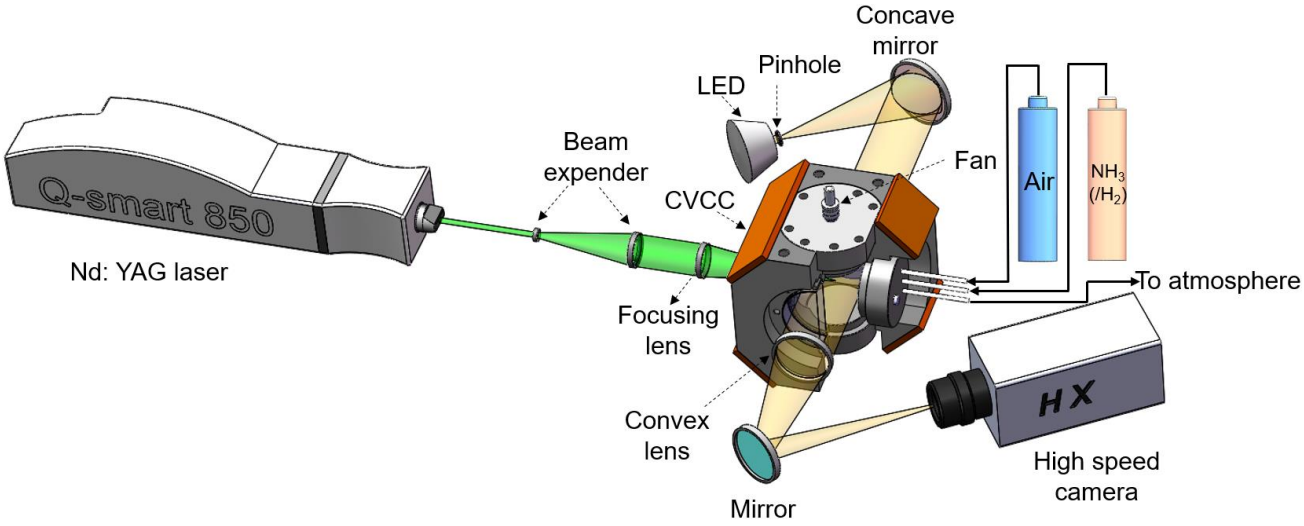

Fig. 1. Schematic of the experimental setup for the laminar flame developments of the ammonia/hydrogen/air mixtures with the laser ignition.

In the optical system, the Nd: YAG laser (Quantel Q-smart 850) was employed to generate a pulsed light of wavelength of 532 nm (the second harmonic) and pulse width of 5 ns. The laser beam with a diameter of 6.5 mm was expanded to 50 mm by a beam expander to prevent the excessive laser energy density from damaging the optical window, and then passed through a plano-convex lens with a focal length of 200 mm to focus the laser beam into the CVCC to generate plasma. The focal length of focusing lens is 200 mm and focal diameter of the laser beam is about 1 mm. The laser fluence is about 3.2×10^{13} W/m^2. The flame kernel was formed in the premixed combustible mixture and gradually

expanded outward. In the experiment, the energy of the beam before the laser entering the CVCC was 220 mJ in average, which can provide reliable optical breakdown in the range of working conditions of this study. During the combustion processes, a piezo-electric transducer (KISTLER 6125C) with a data acquisition instrument was employed to record the dynamic pressure inside the CVCC. According to the first law of thermodynamics and the ideal gas equation, the heat release rate during the combustion in the CVCC can be calculated by

$$\frac{dQ}{dt} = \frac{1}{\kappa - 1} V_{CVCC} \frac{dp}{dt} \tag{1}$$

where Q is the apparent heat released during the combustion; κ is the isentropic index, which is available on the NIST website [33]; V_{CVCC} is the volume of the CVCC, and p is the real-time ambient pressure in the CVCC.

The shadowgraphs of the laminar flame development processes were recorded by a high-speed camera (NAC MEMRECAM HX-6). In the experiments, the imaging speed of the camera was set to 5000 fps, and the resolution of the pictures was 832 pixels × 832 pixels.

The experimental conditions are listed in Table 1. The experiment was repeated three times under each condition and the averaged data were used in the analysis. After each combustion experiment, the CVCC was evacuated and then filled with air for scavenging.

Table 1. Experimental conditions and imaging parameter settings

Proportion of hydrogen content (%)	0, 10, 20
Equivalence ratio, ϕ (-)	0.7-1.4
Initial ambient pressure, P_0 (MPa)	0.1, 0.3, 0.5
Initial ambient temperature, T_0 (K)	360

Imaging speed (fps)	5000

166 *2.2. Data processing methods*

167 In this study, the laminar burning velocity was derived from spherical flame measurements with
168 the linear extrapolation method to zero curvature. Since the actual flame front is curved, the effect of
169 flame stretching should be taken into account during the flame propagation. The procedure of the flame
170 image processing is as follows.

171 First, the image processing is performed to calculate the equivalent radius r_f of the flame. As shown
172 in Fig. 2, since the flame kernel formed after the laser ignition is usually three-lobe or two-lobe shaped,
173 three different methods are used in the present study to calculate the equivalent radius.

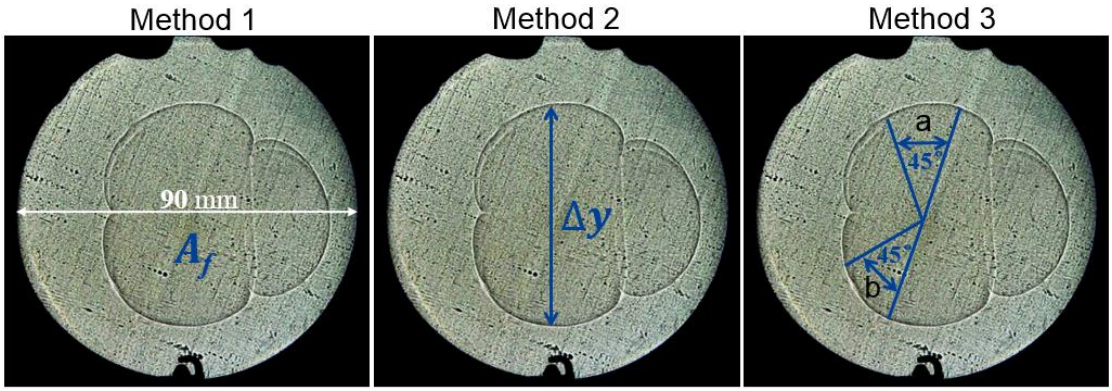

174

175 **Fig. 2.** Schematic diagram of the equivalent radius calculation principle.

176 The first is the equivalent area method. The projection area of burned zone (A_f) is firstly calculated
177 by image processing. Then, the radius of the equivalent circle, r_f, is derived by $r_f = (A_f / \pi)^{0.5}$. To avoid
178 the ignition impact on the flame development at the initial stage, as well as the buoyancy effect and
179 the limiting effect by the vessel wall at the later stage, the image with an equivalent radius of 8-20 mm,
180 termed as quasi-steady state for flame propagation, is processed in this paper [34-36].

181 The second method is to calculate the distance between the top and bottom of the flame kernel as
182 shown in Fig. 2, and then the equivalent radius, $r_f = \Delta y/2$.

The third method is to use the radius of the curvature of a local place on the front surface of the flame as the equivalent radius. As shown in Fig. 2, two certain places a and b are selected for comparative analysis. For better comparison, the ranges of flame kernel development time in the method 2 and the method 3 are consistent with that of the method 1.

Once the equivalent radius is obtained, the stretched flame speed (S_b) can be calculated by the change rate of the equivalent radius with time:

$$S_b = \frac{dr_f}{dt} \tag{2}$$

The stretch rate of the flame (ε) characterizes the change rate of the projection area of the burned zone:

$$\varepsilon = \frac{1}{A_f} \cdot \frac{dA_f}{dt} = \frac{2}{r_f} \cdot \frac{dr_f}{dt} \tag{3}$$

The relationship between the unstretched flame speed (S_b^0) and the stretched flame speed (S_b) can be expressed by

$$S_b^0 - S_b = L_b \cdot \varepsilon \tag{4}$$

The proportional constant L_b in the above formula is the Markstein length. Therefore, S_b^0 can be obtained by the linear extrapolation using the progressive analysis [37, 38]. When ε approaches 0, S_b is nearly equal to S_b^0.

Finally, the laminar burning velocity can be calculated by multiplying the unstretched flame speed with the ratio of the burned gas density to the unburned gas density:

$$S_L = S_b^0 \cdot \frac{\rho_b}{\rho_u} \tag{5}$$

The uncertainty in the stretch extrapolation can be coupled with the uncertainties caused by ignition, radiation, and confinement effects [39]. The flame is in an unstable state at the early stage, and the stretched speed subjects to great effects caused by the ignition. Bradley et al. [34, 35] suggested that the ignition effects can be avoided when the flame radius are larger than 6 mm. Accordingly, the selected smallest radius here is 8 mm. In addition, to reduce the effect of wall confinement, the largest flame radius is limited at 20 mm [36]. Fig. 3 shows the temporal evolution of the equivalent radius change for three methods. Flame propagation is in a quasi-steady state with an equivalent radius of 8-20 mm.

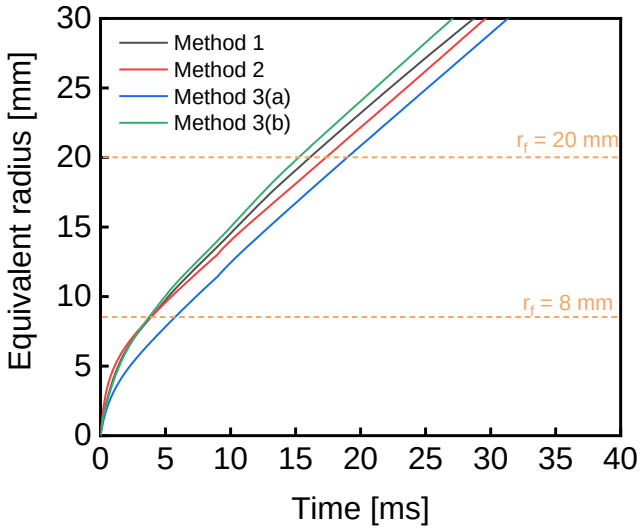

Fig. 3. Development of the equivalent radius of three methods for the combustion of the ammonia/air mixtures (ϕ = 1.0, P_0 = 0.1 MPa, T_0 = 360 K).

2.3. Numerical simulation methods

In this study, a freely propagating adiabatic, premixed, planar flame of the ammonia/hydrogen/air mixtures was simulated using the one-dimensional freely propagating laminar flame model in the CHEMKIN-pro software. Six different chemical reaction mechanisms were adopted in the simulation, including the ammonia chemical reaction kinetic models published by Miller et al. [8], Bian et al. [9],

Okafor et al. [12], Mei et al. [13], Shrestha et al. [14] and the GRI 3.0 mechanism [40]. The corresponding Gas-Phase Kinetic File, Thermodynamics Data File and Gas Transport Data File of the above six kinetic models were used in the simulations.

The operating conditions of the simulations were set the same as those of the experiments, as shown in Table 2. Table 2 also lists some relevant physical characteristics of the ammonia/hydrogen/air mixtures under each operating condition. λ, C_p, α and ν are the thermal conductivity, specific heat at constant pressure, thermal diffusivity, and kinematic viscosity, respectively. ρ_u and ρ_b are the density of unburned gas and the density of burned gas, respectively. For single species, the Lewis number can be calculated by

$$Le_i = \frac{\lambda}{\rho_u C_p D_m} \tag{6}$$

where D_m is the diffusion coefficient of insufficient reaction material (lean or rich mixture). For a mixture of a single component fuel and an oxidizer, Le is defined based on the deficient reactant as the ratio of the thermal diffusivity of the mixture to the molecular diffusivity of the deficient reactant in the mixture. According to Bechtold et al. [41], Le is given by

$$Le = 1 + \frac{\left(Le_E - 1\right) + \left(Le_D - 1\right) A}{1 + A} \tag{7}$$

where $A = 1 + Ze\ (\phi - 1)$. The Lewis numbers Le_E and Le_D are those defined based on the excess reactant and the deficient reactant, respectively.

Ze is the Zel'dovich number which is obtained from

$$Ze = 4\frac{T_{ad} - T_u}{T_{ad} - T_{inner}} \tag{8}$$

where T_{ad} and T_{inner} are the adiabatic flame temperature and the inner layer temperature, respectively.

The geometrical definition of the inner layer temperature was employed in obtaining the values

of T_{inner} for each mixture. Goey et al. [42] suggested that values of T_{inner} can be obtained based on the geometrical definition.

For two-component fuels, this paper adopts the effective Lewis number (Le_{eff}) of multi-component fuels based on the volume weighting calculation [43]:

$$\frac{1}{Le_{eff}} = \frac{X_{NH_3}}{Le_{NH_3}} + \frac{X_{H_2}}{Le_{H_2}} \tag{9}$$

where X_{NH3} and X_{H2} are the volume fractions of ammonia and hydrogen in the mixed fuel, and Le_{NH3} and Le_{H2} are the Lewis numbers corresponding to ammonia and hydrogen, respectively.

The thermal expansion rate, σ, characterizes the ratio of burned gas density to the unburned gas density, which indicates the density fluctuation on both sides of the flame front:

$$\sigma = \frac{\rho_b}{\rho_u} \tag{10}$$

In addition, δ is the thermal diffusion flame thickness [44], which can be calculated by

$$\delta = \frac{\lambda}{\rho_u C_p S_L} = \frac{\alpha}{S_L} \tag{11}$$

In Table 2, the initial ambient pressure, initial ambient temperature and equivalence ratio are the input parameters for the simulations. ρ_u, ρ_b, λ, C_p, α and ν can be calculated by CHEMKIN-pro. The mechanism by Mei et al. [13] was used here. Le and δ can be obtained by further calculations with the above simulation results.

Table 2. Physical characteristics of the ammonia/hydrogen/air mixtures

X_{H2} (%)	P_0 (MPa)	ϕ (-)	ρ_u (kg/m^3)	ρ_b (kg/m^3)	λ (10^{-2}W/m/K)	C_p (W/kg/K)	ν (10^{-5}m^2/s)	α (10^{-5}m^2/s)	Le_{eff}	σ (-)	δ (10^{-4}m)
0	0.1	0.7	0.911	0.178	3.16	1140	2.19	3.04	0.861	5.12	8.86
	0.1	0.8	0.903	0.164	3.18	1156	2.19	3.04	0.927	5.51	5.63
	0.1	0.9	0.896	0.153	3.19	1171	2.19	3.04	0.959	5.86	4.15

	0.1	1	0.889	0.145	3.20	1186	2.19	3.04	0.978	6.13	3.26
	0.1	1.1	0.882	0.144	3.22	1200	2.19	3.04	0.991	6.13	2.68
	0.1	1.2	0.876	0.145	3.23	1214	2.19	3.03	0.999	6.04	2.71
	0.1	1.3	0.87	0.147	3.24	1228	2.19	3.03	1.005	5.92	2.99
	0.1	1.4	0.864	0.149	3.25	1241	2.19	3.03	1.009	5.80	3.41
	0.3	1	2.667	0.432	3.20	1186	0.73	1.01	0.978	6.17	1.40
	0.5	1	4.45	0.718	3.20	1186	0.44	0.61	0.978	6.20	0.94
10	0.1	1	0.875	0.144	3.43	1199	2.24	3.26	0.713	6.08	2.66
	0.3	1	2.63	0.428	3.43	1199	0.74	1.09	0.713	6.14	1.18
	0.5	1	4.38	0.712	3.43	1199	0.45	0.65	0.713	6.15	0.80
20	0.1	0.5	0.913	0.216	3.37	1120	2.24	3.30	0.213	4.23	15.71
	0.1	0.6	0.9	0.192	3.45	1141	2.25	3.36	0.232	4.69	7.39
	0.1	0.7	0.89	0.175	3.51	1160	2.26	3.40	0.275	5.09	4.48
	0.1	0.8	0.88	0.161	3.56	1178	2.27	3.43	0.312	5.47	3.19
	0.1	0.9	0.87	0.15	3.61	1196	2.28	3.47	0.399	5.80	2.51
	0.1	1	0.861	0.142	3.66	1213	2.28	3.51	0.447	6.06	2.08
	0.1	1.1	0.852	0.141	3.71	1230	2.29	3.54	0.478	6.04	1.86
	0.1	1.2	0.844	0.14	3.76	1247	2.30	3.57	0.500	6.03	1.89
	0.1	1.3	0.836	0.141	3.80	1263	2.31	3.60	0.517	5.92	2.04
	0.1	1.4	0.828	0.143	3.84	1279	2.32	3.63	0.530	5.79	2.27
	0.1	1.5	0.821	0.144	3.89	1294	2.32	3.65	0.541	5.70	2.57
	0.3	1	2.58	0.423	3.66	1213	0.76	1.17	0.447	6.10	0.97
	0.5	1	4.3	0.705	3.66	1213	0.46	0.70	0.447	6.10	0.66

3. Results and discussion

3.1. Flame morphology

Fig. 4(a) shows the flame evolutions for the three fuels with different hydrogen fractions under P_0 of 0.1 MPa. The flame kernel has a three-lobe shape and gradually spreads outward. At a fixed moment, the higher the hydrogen proportion, the farther the flame spreads. Among them, the fuel with a hydrogen content of 20% spreads fastest. The flame front is close to the vessel wall at 20 ms. Fig. 4 (b) shows the development of the flame in the ammonia/air mixtures under different initial ambient pressures. With the initial ambient pressure increasing, the flame propagation is slower.

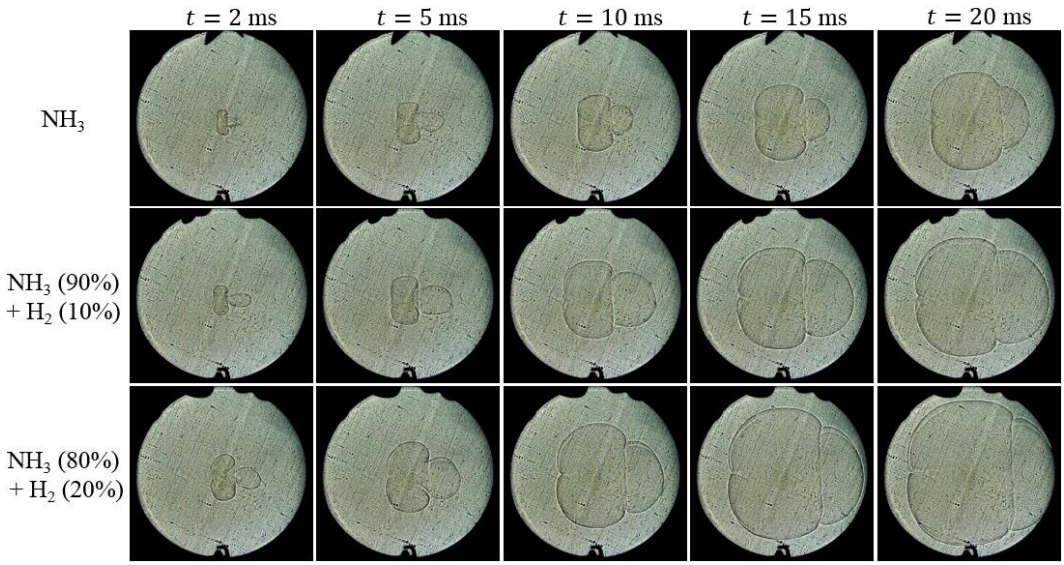

Fig. 4 (a). Temporal development of the flame for the three fuels (ϕ = 1.0, P_0 = 0.1 MPa, T_0 = 360 K).

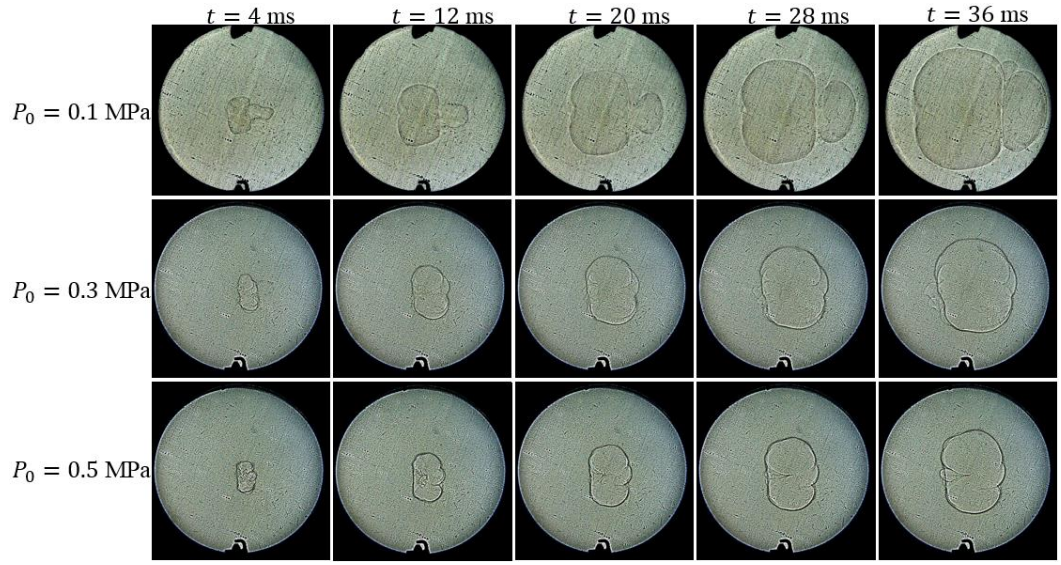

Fig. 4 (b). Temporal development of the flame in the ammonia/air mixtures under different initial ambient pressures (ϕ = 1.0, T_0 = 360 K).

Fig. 5 (a) & (b) shows the development of the projection area of the burned zone and the equivalent radius under different experimental conditions, respectively. It can be seen that the projection area of the burned zone and the equivalent radius is positively correlated with the hydrogen proportions, and negatively correlated with the initial ambient pressures at a fixed moment. When the proportion of hydrogen contents is higher and the initial ambient pressure is lower, the flame kernel spreads faster.

When the projection area of the burned zone increases to 4000 mm^2, the flame front surface approaches the wall of the CVCC.

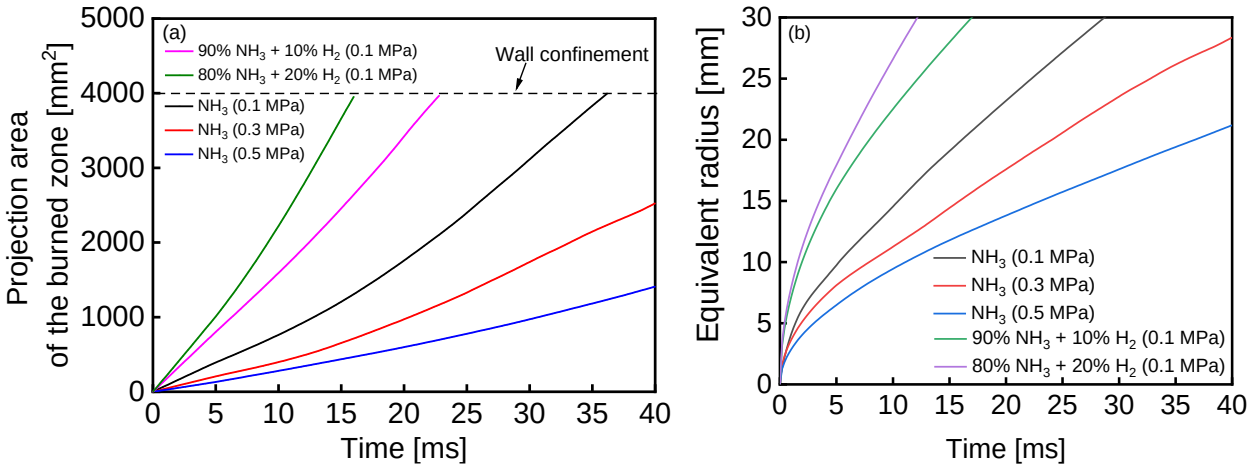

Fig. 5. Development of the projection area of the burned zone (a) and equivalent radius (b) for the combustion of the ammonia/hydrogen/air mixtures under different initial ambient pressures (ϕ = 1.0, T_0 = 360 K).

As shown in Fig. 6, the cellular instability of laminar flame was observed in this study. Two kinds of instabilities are probably involved here: 1) the diffusion-thermal instability and 2) the hydraulic instability [44, 45]. The diffusion-thermal instability can be evaluated by the Lewis number [46]. When *Le* is less than a certain critical value (slightly less than 1), the thermal diffusion at the front of the flame is weaker than the mass diffusion, and the flame propagation is prone to instability. The hydraulic instability is caused by the inconsistent density on both sides of the flame front [45]. When the density of the unburned area and the burned area fluctuate greatly and the thickness of the flame is thinner, the front of the flame is easily disturbed and wrinkles appear [47]. At the initial stage of the flame development, due to the small radius of the flame kernel and the large stretching rate, the flame front surface is affected by the strong curvature limitation and stretched effect, and it tends to stability [44], while the diffusion-heat instability and hydraulic instability are limited [48].

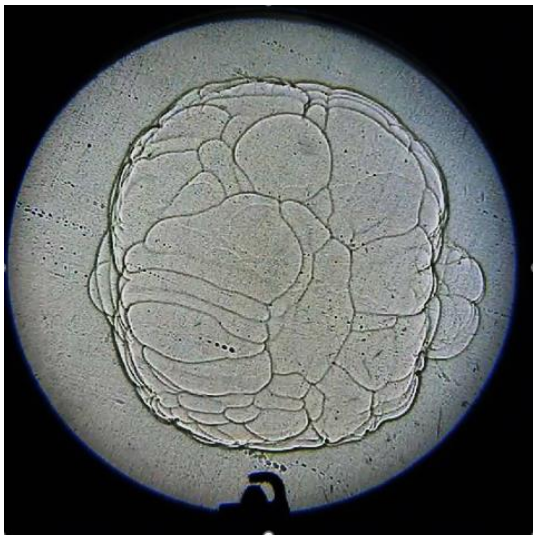

Fig. 6. Cellular instability of the laminar flame in this study (X_{H2} = 20%, P_0 = 0.1 MPa, ϕ = 1.0, t = 35 ms).

In this study, the simulation results of the Lewis number *Le* and flame thickness δ are given in Table 2. When the equivalence ratio is 1.0, for the same fuel, the corresponding *Le* is the same under different pressures, indicating that the effect of diffusion-thermal instability is the same. The thermal expansion rate characterizes the ratio of the density of unburned gas to the density of burned gas. With the initial ambient pressure increasing, the thermal expansion rate does not change much, while the flame thickness will decrease, making it more susceptible to hydraulic instability. In addition, for three different fuels, the flame thickness decreases as the hydrogen proportion increases with the same initial ambient pressure and equivalence ratio, making it more prone to instability.

In this study, the instability was observed at the later stage of flame development when the initial ambient pressure was 0.5 MPa and the proportion of hydrogen contents was 20% as shown in Fig. 7. Since this kind of cellular instability occurred at the later stage of flame development, the equivalent radius of the flame kernel was large at that time. In the range of the equivalent radius from 8 to 20 mm,

the flame instability is limited, and the above methods can be used to calculate the laminar burning velocity.

3.2. Pressure trace and heat release rate

Fig. 7 show the pressure traces and heat release rates during the combustion of the ammonia/hydrogen/air mixtures, respectively. After the mixture is ignited, the flame spreads outward. The fuel burns and begins to release heat, and the pressure in the CVCC gradually rises. When the pressure reaches the peak, the heat releasing process ends. The peak pressure increases as the initial ambient pressure increases for the ammonia/air mixtures as shown in Fig. 7(a). For the fuels with different proportions of hydrogen contents, the higher the hydrogen fraction, the higher the pressure peaks during the combustion process, and the shorter the time it takes to rise to the peak. This can be attributed to the stronger combustion intensity of hydrogen. It is worth noting that at 0-20 ms after the ignition, the pressure in the CVCC increases below 5% of the peak pressure. Therefore, the pressure during this period can be approximated as constant. This time period is also the stage of data processing in this paper.

As shown in Fig. 7(b), the duration of heat releasing increases with the initial ambient pressure increasing. This is caused by the increase in the total amount of reactants and the slow flame propagation speed under the higher initial pressure. In addition, owing to the higher chemical reactivity of hydrogen, when the hydrogen fraction is higher, the heat releasing process is faster. According to the NIST website [33], here the value of the isentropic index (κ), is 1.271, 1.284 or 1.296 in Eq. (1) when the proportion of hydrogen contents in the fuel blends is 0, 10% or 20%, respectively. When the temperature changes in the range of 360 K to 2000 K, the change of the isentropic index is below 7%.

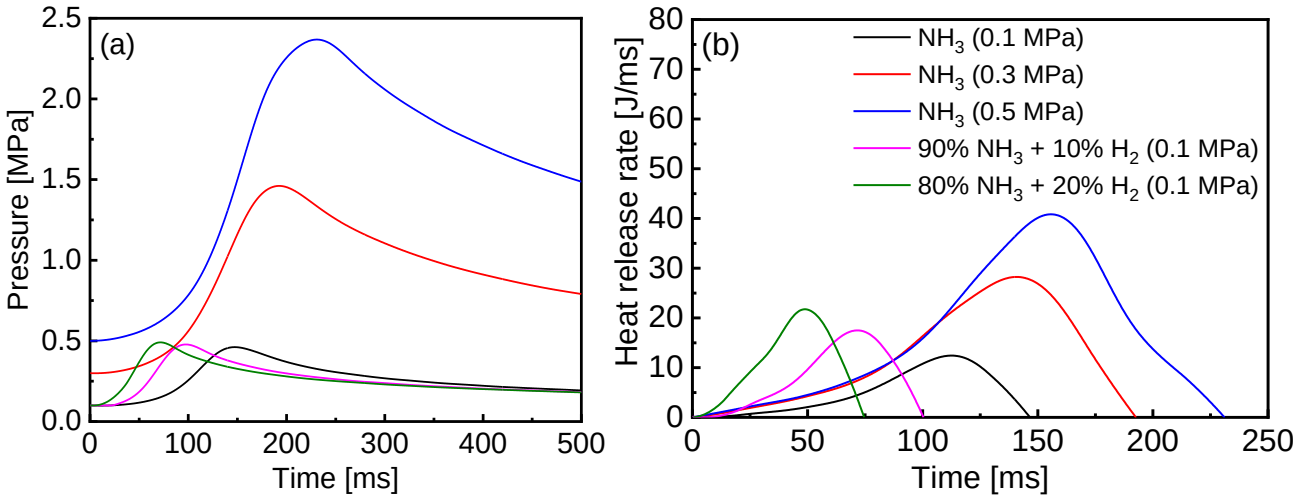

Fig. 7. Pressure change (a) and Heat release rate change (b) in CVCC during the combustion of the ammonia/hydrogen/air mixtures under different initial ambient pressures (ϕ = 1.0, T_0 = 360 K).

3.3. Laminar burning velocity

3.3.1 Effects of equivalence ratio

Fig. 8(a) shows the laminar burning velocities of the ammonia/air mixtures with various equivalence ratios. Plotted are four kinds of results obtained by the proposed methods based on the experimental data of this research. The initial ambient pressure is 0.1 MPa and the initial ambient temperature is 360 K. There are some variations in the laminar burning velocity at the fixed equivalence ratio for the three data processing methods. These variations by different processing methods in this study are well in the range of the variation of the laminar burning velocity at fixed equivalence ratio in the literatures [13, 21, 23, 25, 28] where the electric spark was used to generate a spherical flame to evaluate the laminar burning characteristics. The entire flame front was considered in method 1, which averaged the results of all locations, while method 2 and method 3 were just based on the local place on the front surface of the flame. The error bars, i.e., the standard deviation, of the data by the method 1 are relatively small compared to other methods. Therefore, it is used for comparison and discussion in the following paragraphs.

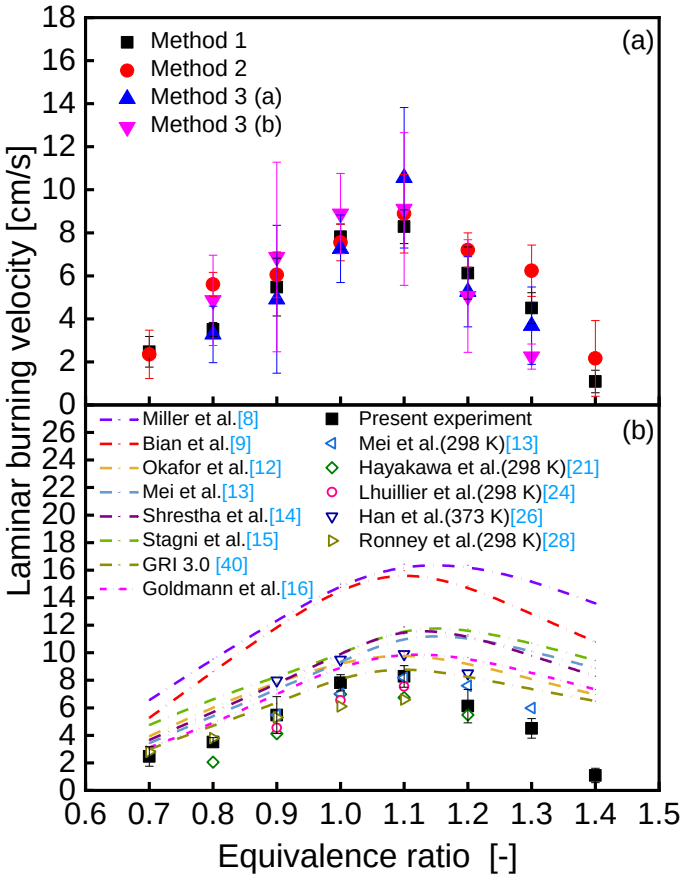

Fig. 8. Laminar burning velocity of the ammonia/air mixtures under various equivalence ratios (P_0 = 0.1 MPa and T_0 = 360 K). Symbols refer to the experimental results in this paper and in previous studies [13, 21, 24, 26, 28]. Lines are the simulation results using different kinetic models [8, 9, 12-15, 40] and calculation results by the correlations of Goldmann et al. [16].

Fig. 8(b) includes the experimental results of the laminar burning velocities of this research, as well as the experimental results of Hayakawa et al. [21], Mei et al. [13], Lhuillier et al. [24], Han et al. [26] and Ronney et al. [28]. Plotted in Fig. 8(b) are also the simulation results using the reaction mechanisms by Miller et al. [8], Bian et al. [9], Okafor et al. [12], Mei et al. [13], Shrestha et al. [14], Stagni et al. [15] and the GRI 3.0 mechanism [40], respectively. The laminar burning velocity correlations developed by Goldmann et al. [16] is also included here based on the present experimental conditions. As the equivalence ratio increases, all the laminar burning velocities obtained by either the

experiments or simulations increase at first, reach peaks around ϕ of 1.1, and then decrease. The experimental peak laminar burning velocities are less than 9 cm/s and lower than most hydrocarbon fuels. According to the Arrhenius dynamics, the laminar burning velocity is mainly affected by the adiabatic flame temperature, and the trend of both of them versus equivalence ratio is almost identical [50].

The simulations using different mechanisms lead to rather large variations at the fixed equivalence ratio, though the general trend of the laminar burning velocity for various equivalence ratios is similar. The kinetic models of Miller et al. [8] and Bian et al. [9] lead to great overpredictions for all the equivalence ratios. The calculation using the GRI 3.0 mechanism shows the best agreement with the experimental results among the existing mechanisms for the equivalence ratios below 1.1. For richer mixtures, however, all the mechanisms as well as the correlations by Goldmann et al. [16] remarkably overpredict the experimental results. Particularly, at the equivalence ratio of 1.4, the GRI 3.0 mechanism overpredicts by a factor of 6. Therefore, the chemical reaction mechanism of ammonia combustion, especially at higher equivalence ratios than stoichiometric, needs to be further improved based on the experimental data.

As the spherical flame spreads outwardly, the radiation effects should be taken into account because it affected the laminar burning velocity. The flame temperature was influenced by the thermal and flow effect induced by radiation and thus the spherical flame propagation speed was reduced by the radiation cooling [49]. The following empirical correlation proposed by Yu et al. [49] can quantify radiation-induced reduction in laminar burning velocity:

$$RL=0.82\left(\frac{S_L}{S_i}\right)^{-1.14}\left(\frac{T_u}{T_i}\right)\left(\frac{P}{P_i}\right)^{-0.3} \tag{12}$$

where S_i = 1 cm/s, T_i = 298 K, and P_i = 101325 Pa. For the experimental peak laminar burning velocity in the present work, the radiation loss was 8.93%. Therefore, the laminar burning velocity under the adiabatic conditions can be obtained after compensating for the radiation loss and it was 9.02 cm/s that is 8.21% higher than the uncorrected value.

Fig. 9 shows the results of the laminar burning velocity changing with the equivalence ratio for the fuel of 80% ammonia and 20% hydrogen. The initial ambient pressure is 0.1 MPa and the initial ambient temperature is 360 K. The error bar is relatively large for ϕ of 1.0 and 1.1, which may be related to the instability of the laminar flame when the laminar burning velocity is fast for the thermal expansion rate, σ, is relatively large. Plotted in Fig. 9 are also for the simulation results using the reaction mechanisms. As the equivalence ratio increases, the laminar burning velocities of the ammonia/hydrogen/air mixtures show a similar trend with the ammonia/air mixtures. When the equivalence ratio is below 0.6, the simulations by all the kinetic models underpredict the experimental results, while most of these models lead to overpredictions for the equivalence ratio above 1.2. For the equivalence ratios from 0.7 to 1.1, the models by Mei et al. [13] , Shrestha et al. [14] and Goldmann's correlations [16] exhibit the better predictive performance than the others.

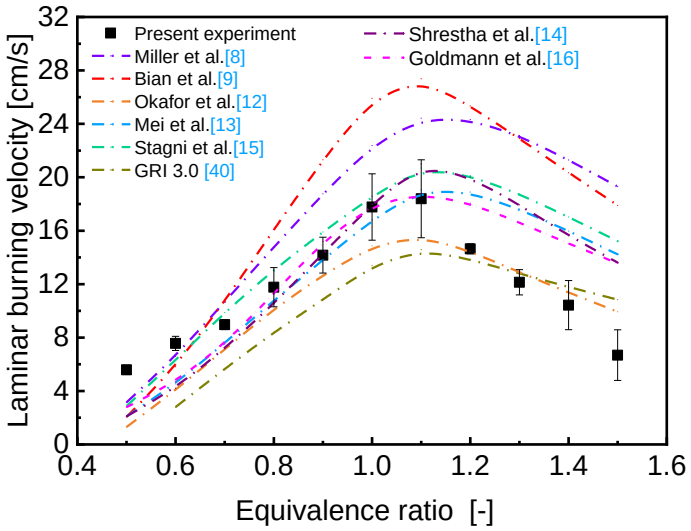

Fig. 9. Laminar burning velocity of the ammonia/hydrogen/air mixtures under various equivalence ratios (X_{H2} = 20%, P_0 = 0.1 MPa and T_0 = 360 K). Symbols refer to the experimental results in this study while lines are the simulation results using different kinetic models [8, 9, 12-15, 40] and the calculation results by the correlations of Goldmann et al. [16].

3.3.2 Effects of initial ambient pressure

Fig. 10 shows the laminar burning velocity under various initial ambient pressures with ϕ of 1.0 and T_0 of 360 K for the three fuels. Also shown are the results by Hayakawa [21] and Ichikawa et al. [23] for comparison. The higher initial ambient temperature in the present experiments, i.e., 360 K, than 298 K in Hayakawa's work, lead to the higher laminar burning velocity. As shown in Fig. 10, the laminar burning velocity nonlinearly decreases with the initial ambient pressure increasing. According to Law et al. [51], the relationship between the laminar burning velocity and the initial ambient pressure is expressed by

$$S_L \propto P_0^{\frac{n}{2}-1} \tag{13}$$

where n is the order of the total reaction. Since the oxidation reaction of ammonia and hydrogen is mainly affected by the two-body branching and carrying reactions [8, 9, 12-15, 40], for example, O + H_2 = H + OH, when the initial ambient pressure is low, n is close to 2 but less than 2 [50, 51]. With the initial ambient pressure becoming higher, the increase in the three-body termination reactions, for example, O + H + M = OH + M, will make n further reduced [51]. As a result, there is a negative correlation between the laminar burning velocity and the initial ambient pressure.

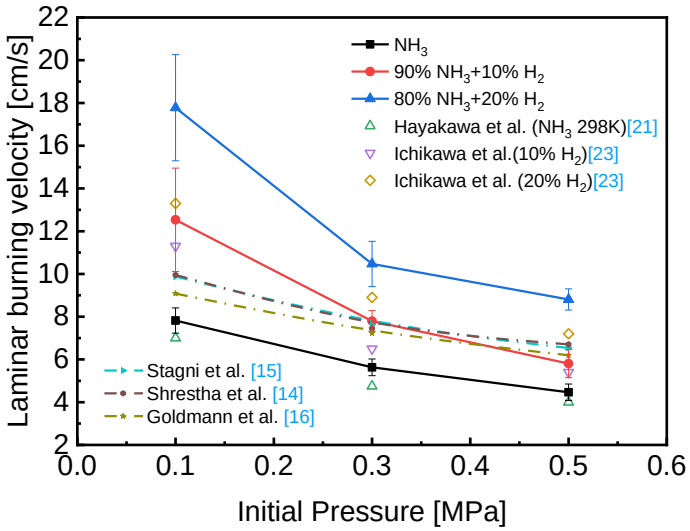

Fig. 10. Laminar burning velocity of the ammonia/hydrogen/air mixtures under various initial ambient pressures (ϕ = 1.0 and T_0 = 360 K). Symbols refer to the experimental results in this paper and in previous studies [21, 23] while lines are the simulation results using different kinetic models [14, 15] and calculation results by the correlations of Goldmann et al. [16].

Table 3 shows the coefficients of the pressure dependence extracted from the experimental or numerical data in Fig. 10. The coefficient of the pressure dependence became smaller when the hydrogen was added based on the present experimental results and such reduction can also be observed from the data by Hayakawa et al. [21] and Ichikawa et al. [23]. In addition, the laminar burning velocity changed more gently with the initial pressure from the simulation results using the mechanisms by Shrestha et al. [14] and Stagni et al. [15]. Considering the experimental conditions of this paper into the correlations in [16], a more gentle coefficient, -0.164, can be obtained. Therefore, the poor performance on the prediction of the coefficient indicates that both the kinetic models and the correlations should be improved.

Table 3. Coefficient of the pressure dependence

NH_3 (present work)	-0.332

90% NH_3+10%H_2 (present work)	-0.461
80% NH_3+20%H_2 (present work)	-0.453
Hayakawa (NH_3) [21]	-0.349
Ichikawa (10%H_2) [23]	-0.475
Ichikawa (20%H_2) [23]	-0.396
Shrestha et al. [14]	-0.251
Stagni et al. [15]	-0.251
Goldmann et al. [16]	-0.164

3.3.3 Effects of hydrogen contents

Fig. 11 shows the experimental and simulation results of the laminar burning velocities varying with the proportion of hydrogen contents under different initial ambient pressures. As shown in the figures, under the three initial pressures, with the hydrogen contents increasing, the laminar burning velocity increases. This confirms that the chemical reactivity of hydrogen is relatively high, and it can significantly accelerate the combustion of ammonia. In the logarithmic graph, the laminar burning velocity and the proportion of hydrogen contents show an approximately linear positive correlation. When the proportion of hydrogen contents reaches 40%, the laminar burning velocity of the ammonia mixtures is comparable to that of methane at the stoichiometric ratio, i.e. 30-40 cm/s.

Regarding the predictability of the existing kinetic models, as shown in Fig. 11(a), the simulation results using Mei et al. [13], Shrestha et al. [14], Stagni et al. [15] mechanism and Goldmann's correlations [16] show the best predictive performance with the experimental values of the ammonia/air mixtures and the ammonia/hydrogen/air mixtures at P_0 of 0.1 MPa, respectively. However, as shown in Fig. 11(b) & (c), with the initial ambient pressure becoming higher, the

simulation results obtained from the seven mechanisms as well as Goldmann's correlations [16] all overpredict the experimental values, indicating that the chemical reaction mechanism of the ammonia/hydrogen oxidation under the high pressures needs to be further revised.

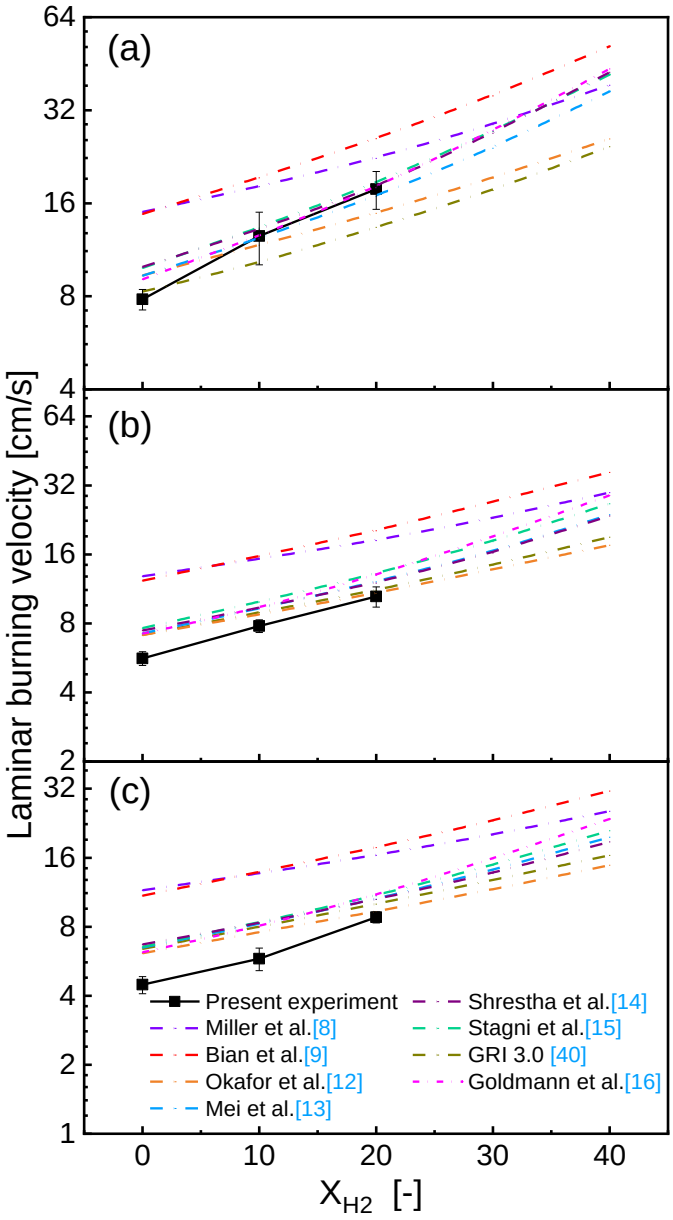

Fig. 11. Laminar burning velocity of the ammonia/hydrogen/air mixtures under various proportions of hydrogen contents. The initial pressure of (a), (b) and (c) are 0.1 MPa, 0.3 MPa and 0.5 MPa, respectively, (ϕ = 1.0 and T_0 = 360 K). Symbols refer to the experimental results in this study and

lines are the simulation results by different kinetic models [8, 9, 12-16, 40] and the calculation results by the correlations of Goldmann et al. [16].

3.4 Flame thickness

Fig. 12 shows the results of the flame thickness under the various initial ambient pressures at ϕ of 1.0. The flame thickness here is calculated by Eq. (11), based on the experimental values of the laminar burning velocity obtained in this work. As shown in Fig. 12, the flame thickness has a negative correlation with the initial ambient pressure as well as the proportion of hydrogen contents. This is also consistent with the previous analysis of flame instability in section 3.1. When the hydrogen fraction and the initial ambient pressure are higher, the flame is more susceptible to the hydraulic instability at the late stages of flame development, resulting in the cellular instability.

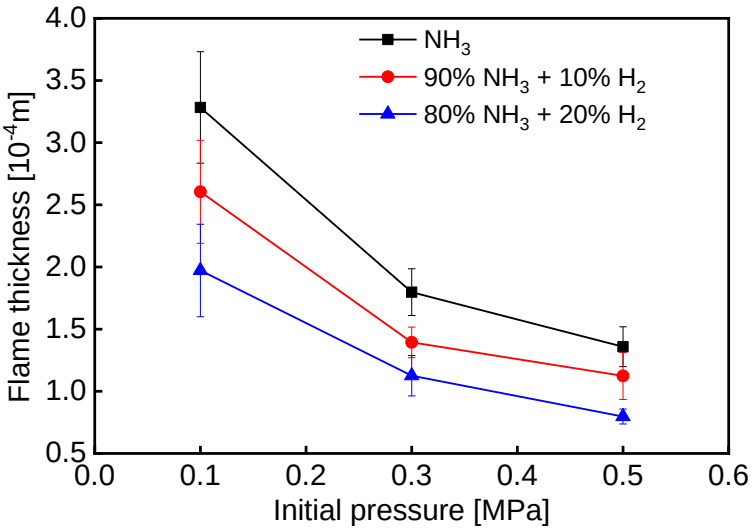

Fig. 12. Flame thickness of the ammonia/hydrogen/air mixtures under various initial ambient pressures for the three fuels (ϕ = 1.0 and T_0 = 360 K). Symbols refer to the experimental results in this study.

4. Summary and conclusions

The laminar burning characteristics of the premixed ammonia/hydrogen/air mixtures have been studied with the experiments and simulations. The effects of equivalence ratio (0.7-1.4), initial ambient pressure (0.1MPa-0.5 MPa), hydrogen fraction (0-20%) on the laminar burning velocity are investigated under the initial ambient temperature of 360K. The major conclusions are summarized as follows:

- The ammonia/air mixtures can be ignited for an equivalene ratio range from 0.7 to 1.4 using laser ignition, and the flame can spread stably.
- The laminar burning velocity of the ammonia/hydrogen/air mixtures increases firstly, reaches the peak at the equivalence ratio around 1.1, and then decreases with the equivalence ratio increasing from 0.7 to 1.4.
- The peak laminar burning velocities of the ammonia/air mixtures are lower than 9 cm/s, which are significantly lower than those of hydrocarbon fuels.
- The simulations using different mechanisms lead to rather large variations at the fixed equivalence ratio, though the general trend of the laminar burning velocity varied with the equivalence ratio is similar. The numerical values of laminar burning velocities are mostly above that of experiments for the ammonia/air mixtures. While the models except for those by Miller and Bian can give reasonable predictions compared to the experimental results for the equivalence ratio from 0.7 to 1.1 in the ammonia (80%)/hydrogen (20%)/air mixtures, all the models overpredict the experiments for the richer mixtures. Therefore, the chemical reaction mechanism of ammonia combustion, especially at the high equivalence ratios, needs to be

further improved. All the experimental results in this paper can be as the data reference for the validation of kinetic models.

- As the initial ambient pressure increases, the laminar burning velocity of the ammonia/hydrogen/air mixtures nonlinearly decreases, and the duration of heat releasing becomes longer.
- The addition of hydrogen can significantly accelerate the laminar burning velocity of the mixtures. The laminar burning velocity and the proportion of hydrogen contents show an approximately linear positive correlation in the logarithmic graph, which provides a data reference for the issue of enhancing the combustion intensity of ammonia.
- The cellular instability can be observed at the late stage of the ammonia/hydrogen/air flames propagation when the proportion of hydrogen contents is 20% and the initial ambient pressure is 0.5 MPa, which is related to the thin flame thickness due to the high hydrogen fraction and the high initial ambient pressure.

Acknowledgements

The supports by the Major International (Regional) Joint Research Project of National Natural Science Foundation of China (52020105009) and the National Natural Science Foundation of China (51776125) are gratefully acknowledged. The assistances by Xinyi Zhou, Xinran Wang and other students in the Large Engine Research Center of SJTU are highly appreciated.

References

[1] Schleussner C-F, Rogelj J, Schaeffer M, Lissner T, Licker R, Fischer EM, et al. Science and policy characteristics of the Paris Agreement temperature goal. Nat Clim Change 2016;6(9):827-35.

[2] Giddey S, Badwal SPS, Munnings C, Dolan M. Ammonia as a Renewable Energy Transportation Media. ACS Sustainable Chem Eng 2017;5:10231-39.

[3] Camilo Casallas, Ibrahim Dincer. Assessment of an integrated solar hydrogen system for electrochemical synthesis of ammonia. Int J Hydrogen Energ 2017; 42(33): 21495-500.

[4] Armijo Julien, Philibert Cédric. Flexible production of green hydrogen and ammonia from variable solar and wind energy: Case study of Chile and Argentina. Int J Hydrogen Energ 2020;45(3):1541-58.

[5] Wang L, Xia M, Wang H, Huang K, Qian C, Maravelias CT, et al. Greening Ammonia toward the Solar Ammonia Refinery. Joule 2018;2(6):1055-74.

[6] Valera-Medina A, Xiao H, Owen-Jones M, David WIF, Bowen PJ. Ammonia for power. Prog Energy Combust Sci 2018;69:63-102.

[7] Kobayashi H, Hayakawa A, Somarathne KDKA, Okafor EC. Science and technology of ammonia combustion. Proc Combust Inst 2019;37(1):109-33.

[8] Miller JA, Smooke MD, Green RM, Kee RJ. Kinetic Modeling of the Oxidation of Ammonia in Flames. Combust Sci Technol 1983;34(1-6):149-76.

[9] Bian J, Vandooren J, Van Tiggelen PJ. Experimental study of the formation of nitrous and nitric oxides in H2−O2−Ar flames seeded with NO and/or NH3. Symp (Int) Combust 1991;23(1):379-86.

[10] Lindstedt RP, Lockwood FC, Selim MA. A Detailed Kinetic Study of Ammonia Oxidation. Combust Sci Technol 1995;108(4-6):231-54.

[11] Tian Z, Li Y, Zhang L, Glarborg P, Qi F. An experimental and kinetic modeling study of premixed NH3/CH4/O2/Ar flames at low pressure. Combust Flame 2009;156(7):1413-26.

[12] Okafor EC, Naito Y, Colson S, Ichikawa A, Kudo T, Hayakawa A, et al. Measurement and modelling of the laminar burning velocity of methane-ammonia-air flames at high pressures using a reduced reaction mechanism. Combust Flame 2019;204:162-75.

[13] Mei B, Zhang X, Ma S, Cui M, Guo H, Cao Z, et al. Experimental and kinetic modeling investigation on the laminar flame propagation of ammonia under oxygen enrichment and elevated pressure conditions. Combust Flame 2019;210:236-46.

[14] Shrestha KP, Lhuillier C, Barbosa AA, Brequigny P, Contino F, Mounaïm-Rousselle C, et al. An experimental and modeling study of ammonia with enriched oxygen content and ammonia/hydrogen laminar flame speed at elevated pressure and temperature. Proc Combust Inst 2020;000:1-12.

[15] Stagni A, Cavallotti C, Arunthanayothin S, Song Y, Herbinet O, Battin-Leclerc F, Faravelli T. An experimental, theoretical and kinetic-modeling study of the gas-phase oxidation of ammonia. React Chem Eng 2020;5:697-771.

[16] Goldmann A, Dinkelacker F. Approximation of laminar flame characteristics on premixed ammonia/hydrogen/nitrogen/air mixtures at elevated temperatures and pressures. Fuel 2018;224:366-378.

[17] Mathieu O, Petersen EL. Experimental and modeling study on the high-temperature oxidation of ammonia and related NOx chemistry. Combust Flame 2015;162(3):554–70.

[18] Hu E, Huang Z, Liu B, Zheng J, Gu X, Huang B. Experimental investigation on performance and emissions of a spark-ignition engine fuelled with natural gas–hydrogen blends combined with EGR. Int J Hydrogen Energ 2009;34(1):528-39.

[19] Pfahl UJ, Ross MC, Shepherd JE, Pasamehmetoglu KO, Unal C. Flammability Limits, Ignition Energy, and Flame Speeds in H2–CH4–NH3–N2O–O2–N2 Mixtures. Combust Flame 2000;123(1-2):140–58.

[20] Takizawa K, Takahashi A, Tokuhashi K, Kondo S, Sekiya A. Burning velocity measurements of nitrogen-containing compounds. J Hazard Mater 2008;155(1-2):144-52.

[21] Hayakawa A, Goto T, Mimoto R, Arakawa Y, Kudo T, Kobayashi H. Laminar burning velocity and Markstein length of ammonia/air premixed flames at various pressures. Fuel 2015;159:98-106.

[22] Xiao P, Wu H, Wang Z, Zhang S, Lee Chia-fon, Wang Z, et al. Experimental and kinetic investigation on the effects of hydrogen additive on laminar premixed methanol–air flames. Int J Hydrogen Energ 2019;44:22263-81.

[23] Ichikawa A, Hayakawa A, Kitagawa Y, Kunkuma Amila Somarathne K D, Kudo T, Kobayashi H. Laminar burning velocity and Markstein length of ammonia/hydrogen/air premixed flames at elevated pressures. Int J Hydrogen Energ 2015;40(30):9570-78.

[24] Lhuillier C, Brequigny P, Lamoureux N, Contino F, Mounaïm-Rousselle C. Experimental investigation on laminar burning velocities of ammonia/hydrogen/air mixtures at elevated temperatures. Fuel 2020;263:116653.

[25] Davis SG, Pagliaro JL, Debold TF, Wingerden M, Wingerden K. Flammability and explosion characteristics of mildly flammable refrigerants. J Loss Prevent Proc 2017;49:662-74.

[26] Han X, Wang ZH, He Y, Liu Y, Zhu Y, Konnov AA. Experimental investigation on laminar burning velocities of ammonia/hydrogen/air mixtures at elevated temperatures. Combust Flame 2020;217:314–20.

572 [27] Zakaznov VF, Kursheva LA, Fedina ZI. Determination of normal flame velocity and critical
573 diameter of flame extinction in ammonia-air mixture. Combust Explos Shock Waves 1978;14:
574 710–13.
575 [28] Ronney PD. Effect of Chemistry and Transport Properties on Near-Limit Flames at Microgravity.
576 Combust Sci Technol 1988;59(1-3):123-41.
577 [29] Dhananjay Kumar Srivastva, Avinash Kumar Agarwal. Laser Ignition of Hydrogen-Air Mixture
578 in a Combustion Bomb. SAE paper 2008-28-0033; 2008.
579 [30] Xu C, Fang D, Luo Q, Ma J, Xie Y. A comparative study of laser ignition and spark ignition with
580 gasoline–air mixtures. Opt Laser Technol 2014;64:343-51.
581 [31] Pal Anuj, KA Avinash. Comparative study of laser ignition and conventional electrical spark
582 ignition systems in a hydrogen fuelled engine. Int J Hydrogen Energy 2015;40(5):2386-95.
583 [32] Liedel G, Schuocker D, Geringer B, Graf J, Klawatsch D, Lenz HP, et al. Laser induced ignition
584 of gasoline direct injection engines. Proceeding SPIE 2005;5777:955-60.
585 [33] NIST, NIST Chemistry WebBook: NIST Standard Reference Database Number 69. <
586 http://webbook.nist.gov/chemistry/>.
587 [34] Bradley D, Gaskell PH, Gu XJ. Burning velocities, Markstein lengths, and flame quenching for
588 spherical methane-air flames: A computational study. Combust Flame 1996;104:176-98.
589 [35] Bradley D, Hicks RA, Lawes M, Sheppard CGW, Woolley R. The measurement of laminar
590 burning velocities and Markstein numbers for iso-octane-air and iso-octane-n-heptane-air mixtures
591 at elevated temperatures and pressures in an explosion bomb. Combust Flame 1998;115:126-44.
592 [36] Burke MP, Chen Z, Ju Y, Dryer FL. Effect of cylindrical confinement on the determination of
593 laminar flame speeds using outwardly propagating flames. Combust Flame 2009;156(4):771-79.

[37] P Clavin. Dynamic behaviour of premixed flame fronts in laminar and turbulent flows, Prog Energy Combust Sci 1985;11:1–59.

[38] Hu E, Huang Z, He J, Zheng J, Miao H. Experimental and numerical study on laminar burning velocities and flame instabilities of hydrogen–air mixtures at elevated pressures and temperatures. Int J Hydrogen Energy 2009;34:8741-55.

[39] Wu F, Liang W, Chen Z, Ju Y, Law CK. Uncertainty in stretch extrapolation of laminar flame speed from expanding spherical flames, Proc Combust Inst 2015;35:663-70.

[40] Frenklach M, Bowman T, Smith G. GRI-Mech 3.0. 2000. <http://www.me.berkeley.edu/gri-mech/index.html>.

[41] Bechtold JK, Matalon M. The dependence of the Markstein length on stoichiometry. Combust Flame 2001;127:1906-1913.

[42] de Goey LPH, Hermanns RTE, Bastiaans RJM. Analysis of the asymptotic structure of stoichiometric premixed CH4–H2–air flames. Proc Combust Inst 2007; 31:1031-1038.

[43] Dinkelacker F, Manickam B, Muppala SPR. Modelling and simulation of lean premixed turbulent methane/hydrogen/air flames with an effective Lewis number approach. Combust Flame 2011; 158:1742-49.

[44] Law CK, Jomaas G, Bechtold JK. Cellular instabilities of expanding hydrogen/propane spherical flames at elevated pressures: theory and experiment. Proc Combust Inst 2005;30(1):159-67.

[45] Bechtold JK, Matalon M. Hydrodynamic and diffusion effects on the stability of spherically expanding flames. Combust Flame 1987;67(1):77-90.

[46] Parlange JY. Influence of Preferential Diffusion on the Stability of a Laminar Flame. J Chem Phys 1968;48(4):1843-49.

[47] Matalon M, Cui C, Bechtold JK. Hydrodynamic theory of premixed flames: effects of stoichiometry, variable transport coefficients and arbitrary reaction orders. J Fluid Mech 2003;487:179-210.

[48] Hu E, Huang Z, He J, Zheng J, Miao H. Measurements of laminar burning velocities and onset of cellular instabilities of methane–hydrogen–air flames at elevated pressures and temperatures. Int J Hydrogen Energy 2009;34(13):5574-84.

[49] Yu H, Han W, Santner J, Gou X, Sohn CH, Ju Y, et al. Radiation-induced uncertainty in laminar flame speed measured from propagating spherical flames. Combust Flame 2014. 161: 2815-24.

[50] Law CK. Combustion physics. Cambridge University Press; 2006, p. 275-82.

[51] Egolfopoulos F, Law CK. Chain mechanisms in the overall reaction orders in laminar flame propagation. Combust Flame 1990;80(1):7-16.

Nomenclature

A_f	projection area of the burned zone [mm^2]
C_p	specific heat at constant pressure [W/kg/K]
E_a	activation energy [J]
H_2	hydrogen
H_2O	water
L_b	Markstein length [cm]
Le	Lewis number [-]
Le_D	Lewis number of the deficient reactant [-]
Le_E	Lewis number of the excess reactant [-]

637 Le_{eff} effective Lewis number [-]

638 Le_i Lewis number of species i [-]

639 n order of the total reaction [-]

640 N_2 nitrogen

641 N_2O nitrous Oxide

642 NH_3 ammonia

643 NO nitric oxide

644 O_2 oxygen

645 CVCC constant volume combustion chamber

646 p real-time ambient pressure in the CVCC [MPa]

647 P_0 initial ambient pressure [MPa]

648 Q apparent heat released during the combustion [J]

649 S_L laminar burning velocity [cm/s]

650 R gas constant [-]

651 RL Radiative loss [%]

652 r_f equivalent radius of the flame [mm]

653 S_b^0 unstretched speed [cm/s]

654 S_b stretched speed [cm/s]

655 T_{ad} adiabatic flame temperature [K]

656 T_0 initial ambient temperature [K]

657 T_{inner} inner layer temperature [K]

658 V_{CVCC} volume of the CVCC [L]

V_{H2}	volume of hydrogen in the mixed fuel [m^3]
X_{H2}	volumetric percentage of hydrogen in the mixed fuel [%]
X_{NH3}	volumetric percentage of ammonia in the mixed fuel [%]
Δy	distance between the top and bottom of the flame kernel [mm]
Ze	Zel'dovich number [-]
α	thermal diffusivity [$10^{-5}m^2/s$]
δ	flame thickness [$10^{-4}m$]
ε	stretch rate of the flame [1/s]
ϕ	equivalence ratio [-]
κ	isentropic index [-]
λ	thermal conductivity [$10^{-2}W/m/K$]
ρ_b	density of burned gas [kg/m^3]
ν	kinematic viscosity [$10^{-5}m^2/s$]
ρ_u	density of unburned gas [kg/m^3]
σ	thermal expansion rate [-]